

Competing Magnetic Ground States in Copper-Doped $\text{Pb}_{10}\text{P}_6\text{O}_{25}$

Lin Hou,^{1,2} Kevin Allen,^{1,3} Christopher Lane,¹ and Jian-Xin Zhu^{4,1}

¹*Theoretical Division, Los Alamos National Laboratory, Los Alamos, New Mexico 87545, USA*

²*Department of Physics and Engineering Physics,
Tulane University, New Orleans, 70118, Louisiana, USA*

³*Department of Physics and Astronomy, Rice University, Houston, 77005, Texas, USA*

⁴*Center for Integrated Nanotechnologies, Los Alamos National Laboratory, Los Alamos, 87545, New Mexico, USA*

(Dated: March 17, 2026)

We investigate the electronic and magnetic properties of copper-doped $\text{Pb}_{10}(\text{PO}_4)_6\text{O}$ using a combination of density functional theory and many-body perturbation theory. The flat half-filled electronic band at the Fermi level is found to give way to an incommensurate antiferromagnetic instability with wave vector $(0.28\pi, \pm 0.47\pi, \pi)$ within the random phase approximation arising predominantly from Cu- d_{yz} and Cu- d_{xz} orbitals. Moreover, the Heisenberg exchange coupling between neighboring copper atoms is estimated to be ~ 1 meV. Our results suggest that magnetism in copper-doped $\text{Pb}_{10}(\text{PO}_4)_6\text{O}$ is localized on the impurity copper site, with no long-range ordering. These findings support the picture that copper behaves as a magnetic impurity within the Pb-apatite matrix.

I. INTRODUCTION

Flat band systems have recently garnered significant attention as a platform for realizing emergent quantum phases of matter. The negligible band dispersion in these systems yields a nearly infinite effective mass and a large density of states (DOS) near the Fermi level. Consequently, strong correlation effects are readily amplified to drive emergent phenomena, with experimental reports including Fractional Chern insulators¹, fractional quantum anomalous Hall^{2,3}, unconventional superconductivity⁴⁻⁶, strange metals⁷, and non-Fermi liquid behavior⁸.

Magnetism also naturally arises from flat band dispersions owing to the large DOS which promotes spontaneous spin polarization and lowers the total energy of the system. However, very few material examples have been realized that host flat band driven states. At present, examples are limited to the Kagome family of compounds⁹⁻¹¹, with Lieb lattice predictions suggesting flat band boosted ambient temperature ferromagnetism in the 2D limit¹². These few instances give us a glimpse into the vast phase space of possibilities and call for further exploration of new materials.

Recently, Lee et al.^{13,14} reported a possible room-temperature and atmospheric-pressure superconductor in a copper-doped lead apatite crystal, $\text{Pb}_{10-x}\text{Cu}_x(\text{PO}_4)_6\text{O}$ for $0.9 < x < 1.1$, known as LK-99. This announcement attracted great attention that spurred numerous experimental and theoretical groups worldwide to attempt to replicate this extraordinary claims¹⁵⁻³⁶. The experimental efforts have faced significant challenges in reproducing the synthesis and observations of Lee et al., with a few studies still on-going^{37,38}.

In parallel, the electronic structure of LK-99 was explored in a number of theoretical studies²⁶⁻³⁶. Interestingly, replacing one Pb atom with that of copper transforms the electronic states of lead apatite, yielding a very narrow half-filled band at the Fermi level³⁹, thereby hinting at the potential for emergent strong cor-

relation effects. By applying density functional theory (DFT) calculations with a Hubbard U , one found ferromagnetic (FM) and A-type antiferromagnetic (AFM-A) states³². Additionally, when spin-orbit coupling (SOC) is included, the flat band splits revealing Weyl nodes at the Fermi level, suggesting LK-99 to be a Weyl semimetal^{40,41}. Beyond DFT calculations have focused on examining correlation corrections to the electronic band structure and possible pairing scenarios⁴²⁻⁴⁹. While the condensed matter community has failed to confirm any of the alleged superconducting properties, the very narrow flat bands at the Fermi level are intriguing and motivate further theoretical study.

In this work, we investigate the electronic and magnetic properties of $\text{Pb}_9\text{CuP}_6\text{O}_{25}$ using a combination of density functional theory (DFT) and many-body perturbation theory. Our analysis reveals that $\text{Pb}_9\text{CuP}_6\text{O}_{25}$ is metallic with strong hybridization of Cu- $3d$ and O- $2p$ states near the Fermi level and an incommensurate magnetic instability with a propagation vector of $(0.28\pi, \pm 0.47\pi, \pi)$. Furthermore, we estimate the nearest-neighbor Heisenberg exchange coupling parameters to be quite small, ~ 1 meV. Thus, despite the seductive nature of the flat band, our results suggest that magnetism in $\text{Pb}_9\text{CuP}_6\text{O}_{25}$ is localized on the impurity copper site, with no long-range ordering. These findings underscore the picture that copper behaves as a magnetic impurity within the Pb-apatite matrix.

II. THEORETICAL AND CALCULATION DETAILS

A. First-principles calculations

Ab initio calculations were carried out by using the pseudopotential projector-augmented wave method^{50,51} implemented in the Vienna *ab initio* simulation package (VASP)^{52,53} with an energy cutoff of 520 eV for the plane-

wave basis set. Exchange-correlation effects were treated using the recently constructed strongly-constrained and appropriately-normed (SCAN) meta-GGA density functional^{54,55}. A $10 \times 10 \times 10$ Γ -centered k mesh was used to sample the Brillouin zone. We substituted a Cu atom for Pb(1) in the pristine crystal structure^{56,57} in accord with the experimental measurements to initialize our calculations. All atomic sites in the unit cell along with the unit cell volume and shape were relaxed simultaneously using a conjugate gradient algorithm to minimize energy with an atomic force tolerance of 0.001 eV/Å and a total energy tolerance of 10^{-6} eV. The resulting lattice parameters a , b , and c are equal to 9.643 Å, 9.643 Å, and 7.233 Å, respectively.

B. Local Projections and Response Function Calculations

The many-body theory calculations of the spin-orbital fluctuations and magnetic instabilities within the random phase approximation (RPA) were performed using real-space local projections, as implemented in VASP⁵⁸. For $\text{Pb}_9\text{Cu}(\text{PO}_4)_6\text{O}$, the full manifold of Cu- $3d$, and the O- p states of the four oxygens with the largest contribution to the electronic density of states around Fermi energy (a total of 17 orbitals) were included in generating the orbital projections.

To calculate the polarizability $\chi_0(\mathbf{q}, \omega)$, we assume a non-interacting ground state, which allows us to replace the dressed single particle Green's function with its non-interacting counterpart,

$$\hat{g}_{\text{KS}}(\mathbf{k}, i\omega) = \sum_n \frac{|\psi_{\mathbf{k}n}^{KS}\rangle \langle \psi_{\mathbf{k}n}^{KS}|}{i\omega - \epsilon_{\mathbf{k}n}} \quad (1)$$

given in the Kohn-Sham basis where n is the band index and \mathbf{k} is the momentum wave vector in the Brillouin zone. To obtain the atomic-orbital resolved single-particle Green's function the Kohn-Sham wave function is projected onto a set of localized atomic-site-, orbital- and spin-dependent basis functions $|\phi_{lm}^{\tau\sigma}\rangle$ ⁵⁹:

$$|\psi_{\mathbf{k}n}\rangle = \sum_{lm\tau} P_{nk\sigma}^{lm\tau} |\phi_{lm}^{\tau\sigma}\rangle \quad (2)$$

where $P_{nk\sigma}^{lm\tau}$ is the overlap between the Kohn-Sham wave function and the local basis set, $\langle \phi_{lm}^{\tau\sigma} | \psi_{\mathbf{k}n} \rangle$. $\hat{g}_{\text{KS}}(\mathbf{k}, i\omega)$ is then projected onto the local basis set as:

$$\begin{aligned} G_0^{\sigma\sigma'}{}_{lm\tau, l'm'\tau'}(\mathbf{k}, i\omega) &\equiv \langle \phi_{lm}^{\tau\sigma} | \hat{g}_{\text{KS}}(\mathbf{k}, i\omega) | \phi_{l'm'}^{\tau'\sigma'} \rangle \\ &= \sum_n \frac{P_{nk\sigma}^{lm\tau} P_{nk\sigma}^{*l'm'\tau'}}{i\omega - \epsilon_{nk}} \end{aligned} \quad (3)$$

This Green's function is analogous to that obtained using a tight-binding Hamiltonian, where the eigenvectors of the Hamiltonian have been replaced by the local projector overlaps. Furthermore, this form allows for the

computation of the non-interacting polarizability:

$$\begin{aligned} \chi_0^{\sigma\sigma'\mu'\nu'\sigma''\mu''}(\mathbf{q}, i\omega_n) &= \\ \frac{1}{N_{\mathbf{k}}} \frac{1}{\beta} \sum_{\mathbf{k}l} G_0^{\sigma\sigma'}{}_{\mu\nu}(\mathbf{q} + \mathbf{k}, i\omega_n + ip_l) G_0^{\sigma''\mu''}{}_{\mu'\nu'}(\mathbf{k}, ip_l) \end{aligned} \quad (4)$$

where $i\omega_n$ and ip_l are Matsubara frequencies, $\beta = 1/k_B T$, T is the temperature and k_B is Boltzmann constant, and $\mu(\nu)$ are composite indices of orbital and atomic site. Using G_0 , the polarizability can be simplified by performing the Matsubara frequency summation and analytically continuing $i\omega_n \rightarrow \omega + i\delta$, for $\delta \rightarrow 0^+$. Implementation details of Eq. (4) are given in Ref.⁶⁰.

To gain insight into the landscape of charge and magnetic instabilities in the ground state, we examine the response ($\delta\rho$) of the system to an infinitesimal perturbing source field ($\delta\pi$). The associated response function in the generalized RPA-type matrix form is given by,

$$\chi^{MN}(\mathbf{q}, \omega) = [1 - \chi_0^{MI}(\mathbf{q}, \omega)v^{IK}]^{-1} \chi_0^{KN}(\mathbf{q}, \omega) \quad (5)$$

where the orbital indices have been suppressed, the spin indices I, J, L, M take the value 0, x , y , or z , v^{ML} is the electron-electron interaction, and the polarizability χ_0 is defined in Eq. 4. To facilitate our analysis, we let

$$\begin{aligned} \bar{F}^{MK}(\mathbf{q}, \omega) &= \chi_0^{MI}(\mathbf{q}, \omega)v^{IK} \\ &= V_{\alpha}(\mathbf{q}, \omega)\Lambda_F^{\alpha}(\mathbf{q}, \omega)V_{\alpha}^{-1}(\mathbf{q}, \omega) \end{aligned} \quad (6)$$

where Λ_F is a diagonal matrix and V is the eigenvectors. Now as $\Lambda_F(\mathbf{q}, \omega = 0)$ approaches 1, χ becomes singular, signaling an instability to an ordered phase with ordering vector \mathbf{Q} .

A $21 \times 21 \times 21$ Γ -centered mesh was used to evaluate the local projectors and the response functions in the Brillouin zone. Only the 8 bands within a 1 eV window about the Fermi level were retained in the band summation in the polarizability. A small broadening $\delta = 0.01$ eV was used with a temperature of $T = 10$ K. Coulomb interactions were included via the multi-orbital Hubbard model on the Cu sites similar to Ref.⁶¹. The maximum instability was found to equal 1 for $U = 0.67$ eV.

III. RESULTS AND DISCUSSION

A. Crystal and Electronic Structure

Figure 1(a) and (b) display the crystal structure in the primitive cell and the first Brillouin zone with the high-symmetry points labeled for $\text{Pb}_9\text{Cu}(\text{PO}_4)_6\text{O}$, respectively. The lattice is made up of layered planes containing Cu, O, P and Pb atoms. In this structure, Cu atoms form one-dimensional chains along the c -axis, connecting through oxygen atoms in a linear arrangement (Cu-O-Cu). Notably, only a single copper atom appears in the unit cell. P and O atoms form phosphate (PO_4) tetrahedrons, which help stabilize the lattice, while Pb

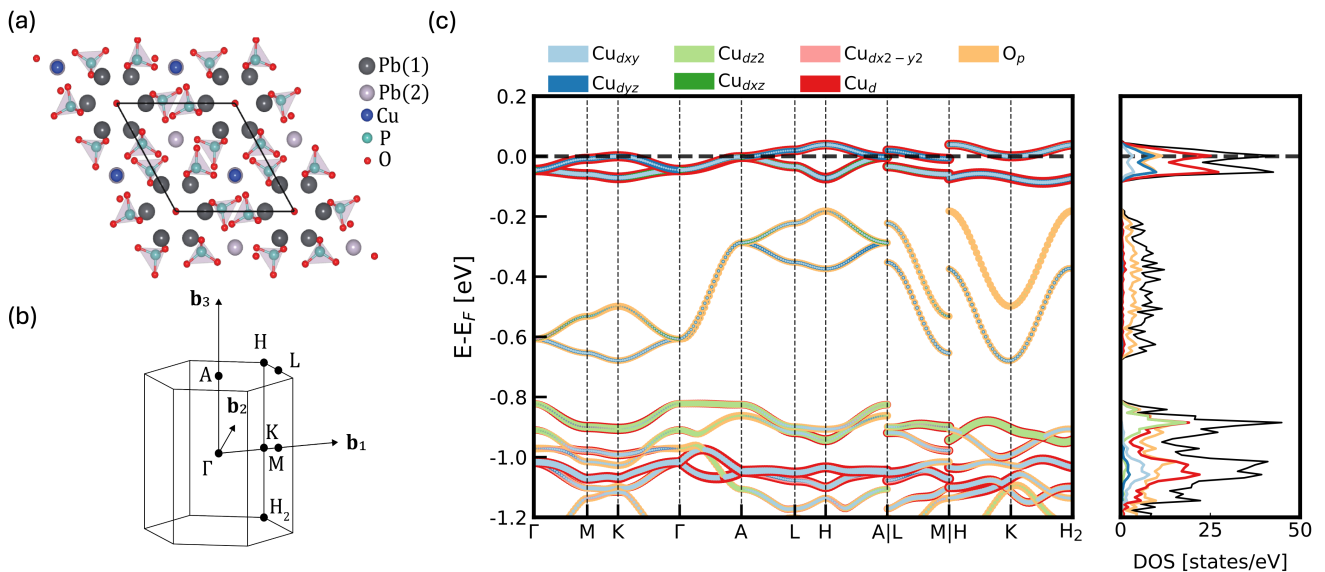


FIG. 1. (a) Crystal structure of $\text{Pb}_9\text{CuP}_6\text{O}_{25}$ viewed along the c -axis. Black lines denote the primitive unit cell. (b) The associated first Brillouin zone with labeled high-symmetry points. (c) Electronic band structure and corresponding density of states for the non-magnetic phase. The size and color of the dots are proportional to the fractional weight of the various indicated site-resolved orbital projections.

atoms occupy sites in a layered arrangement. This structure is built on a trigonal Bravais lattice with P3 symmetry and is non-centrosymmetric.

Figure 1(c) presents the electronic band structure of $\text{Pb}_9\text{CuP}_6\text{O}_{25}$ in the non-magnetic (NM) phase. Strong hybridization between the Cu-3d and O-2p orbitals is observed, where the half-filled antibonding Cu-3d/O-2p band crosses the Fermi level and its bonding partner “bookends” the spectrum from 1.1 eV binding energies. In between, the dispersive electronic states are primarily contributed by O-2p orbitals. The Cu-3d bands are very narrow, especially near the Fermi level. In contrast, the O-2p bands are about twice more dispersive than the Cu-3d bands in the b_1 - b_2 plane, and display strong dispersion along the b_3 axis, as illustrated along the Γ -A, L-M, H-K, and K- H_2 lines in the Brillouin zone. This suggests the Cu-3d electrons are quite localized in the unit cell, whereas the O-2p electrons can readily hop between the Pb layers along the c -axis. The flat bands at the Fermi level arise from the partial (1/4) occupancy of the corner oxygen sites and the hybridization with the Cu-3d orbitals²⁸⁻³⁰.

Typically, when a compound is doped via chemical substitution we witness the appearance of donor/acceptor states as in semiconductors or the addition/subtraction of electrons (holes) from a metallic system resulting in a shift of the Fermi level. Overall, the nature of the electronic states is expected to be adiabatically connected to the parent undoped compound. Here, when a single lead atom is substituted by copper atom, the electronic structure undergoes a dramatic change from an insulator

to a flat band metal. This suggests two pictures, either copper is an impurity that is highly hybridized with the rest of the Pb-apatite system or $\text{Pb}_9\text{CuP}_6\text{O}_{25}$ is the parent compound of a new family of flat band materials with little connection to its insulator ancestor.

B. Magnetic Instabilities

A key consequence of flat bands at the Fermi level is the possible emergence of broken symmetry phases that have the capacity to couple to multiple different degrees of freedom. In $\text{Pb}_9\text{CuP}_6\text{O}_{25}$, reports of magnetism^{20,62-64} are intriguing and are in need for further analysis.

Figure 2 shows the leading instability $\Lambda_F^0(\mathbf{q}, 0)$ for various values of q_z between π and 0 for $\text{Pb}_9\text{CuP}_6\text{O}_{25}$. In panel (a), $\Lambda_F^0(\mathbf{q}_\perp, 0)$ reaches a value of 1 at $\mathbf{Q} = (0.28\pi, \pm 0.47\pi, \pi)$ (white ‘x’). The ordering vectors are incommensurate and lie off of the high-symmetry lines of the Brillouin zone. Moreover, Λ_F^0 is very flat throughout the zone, as indicated by the overlaid contour curves. This flatness suggests that there is a dense manifold of q -vectors that compete with \mathbf{Q} and hint at the presence of magnetic fluctuations in the ground state of $\text{Pb}_9\text{CuP}_6\text{O}_{25}$.

As q_z decreases, the maximum value of Λ_F^0 is reduced with a concomitant contraction of the plateau of instabilities. In Panels (b)-(f), there are three ‘islands’ around the Γ and M points in the Brillouin zone (green shaded regions), whereas in Panels (g)-(k) the instability plateau at the zone center reduces significantly, forming a ring-

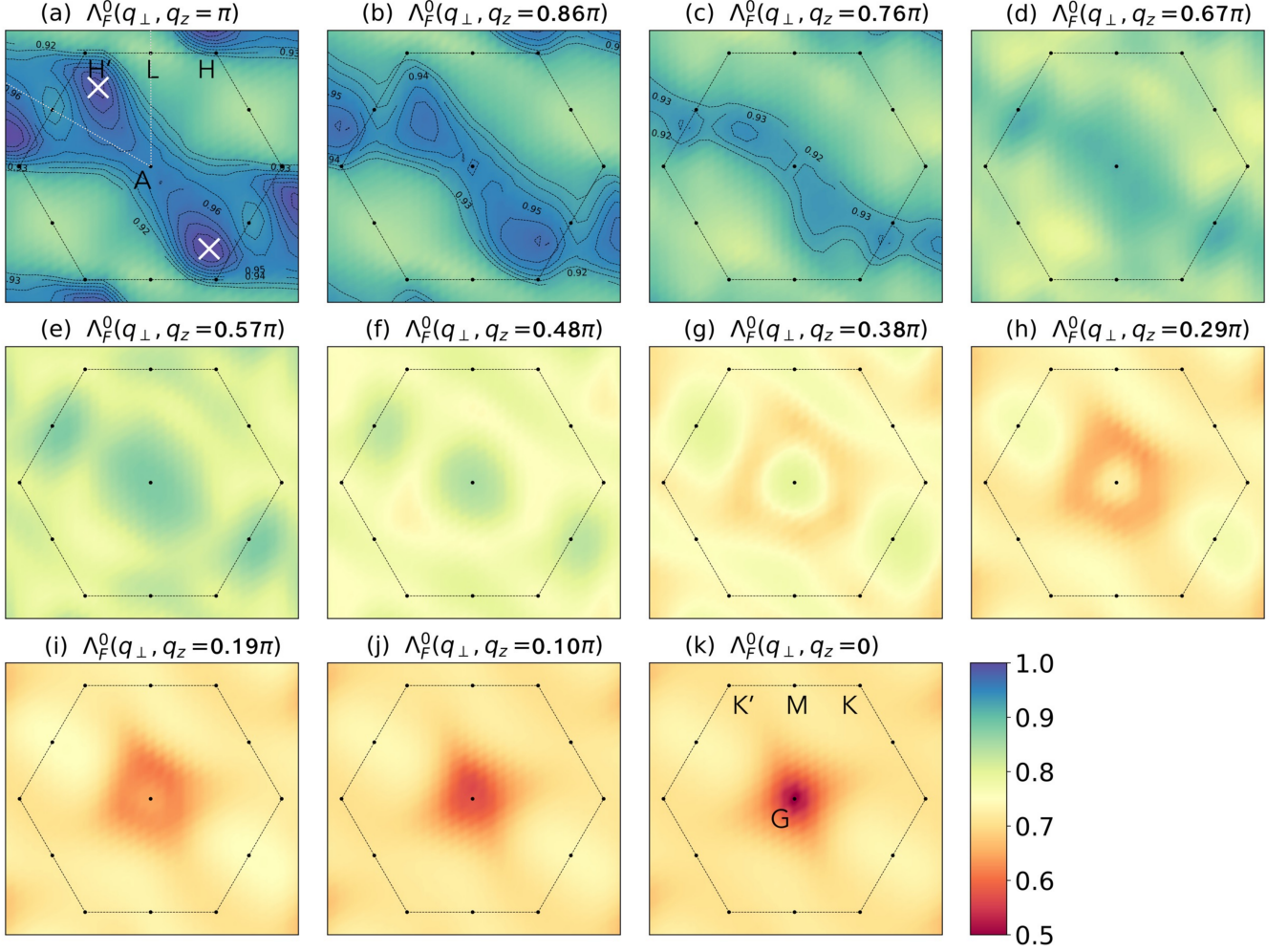


FIG. 2. Momentum dependence of $\Lambda_F^0(\mathbf{q}, \omega = 0)$ for pristine $\text{Pb}_9\text{CuP}_6\text{O}_{25}$ in the non-magnetic phase for various slices along q_z . The white “x” marks denote the critical instability momenta \mathbf{Q} . The black dashed line gives the boundary of the Brillouin zone and the gray dotted lines indicate the reciprocal lattice vectors. The color bar indicates the instability strength.

like structure. Finally, the minimum value of Λ_F^0 is concentrated about Γ , thereby indicating that ferromagnetic (FM) ordering is the least favorable magnetic configuration.

In single crystal samples, no anomalies indicative of phase transitions are observed over a wide range of temperatures up to 800 K, consistent with a fluctuating magnetic state⁶². Since the flat band is extremely sensitive to structural and substitutional disorder, some experiments^{20,62–64} observe a weak ferromagnetism. However, this is likely due to the local magnetic order in inhomogeneous networks of Cu substituents that originates from frustrated exchange interactions⁶².

To quantify the total number of competing magnetic configurations, we introduce the density of instabilities $\lambda(\Omega)$ similar to Ref.⁶⁰, where $\lambda(\Omega)d\Omega$ is the number of instabilities in the system whose strengths lie in the range

from Ω to $\Omega + \delta\Omega$. That is, $\lambda(\Omega)$ is defined as

$$\lambda(\Omega) = \frac{1}{N_{\mathbf{q}}} \sum_{\mathbf{q}\alpha} \delta(\Lambda_F^\alpha(\mathbf{q}, 0) - \Omega) \quad (8)$$

where Ω is the instability strength and α enumerates the instability eigenvalues defined in Eq. 7. We further emphasize that $\lambda(\Omega)$ contains the instability information for all eigenvalues, not just for the maximum.

Figure 3 presents the density of instabilities $\lambda(\Omega)$ for $\text{Pb}_9\text{CuP}_6\text{O}_{25}$, where the colors indicate the contribution of various instability eigenvalues. The total density of instabilities (grey line and shading) displays sharp leading edge near an instability strength of 1.0 arising from the flat region of Λ_F^0 near Q [Fig. 2 (a)-(c)]. The large population of instabilities at the leading edge with different ordering \mathbf{q} -vectors suggests competition between \mathbf{q} -vectors that typically necessitates the inclusion of vertex corrections to capture the low temperature behavior⁶⁵.

A pronounced Van Hove peak appears around $\Omega \sim 0.7$

far from the Fermi level.

In both spin and charge channels, $O-2p$ play a very limited role in the charge/spin fluctuations compared to those from copper. This stems from their very small weight in the electronic structure near the Fermi level and the negligible correlations on the O sites. Moreover, the reduced weight in the charge channel is driven, in part, by the use of the multi-orbital Hubbard model for v . That is, the local nature of v promotes local moment formation by setting an energy penalty for two spin to occupy the same site. In contrast, purely local interactions cannot encourage charge disproportionation since they do not provide any energetic advantage for accumulating (depleting) charge on neighboring atomic sites.

C. Magnetic Exchange Parameters

The fluctuating magnetic state described in the RPA analysis can originate from competition between different long-range magnetic configurations or a simple local impurity, so to distinguish these two scenarios, we estimate the nearest-neighbor exchange coupling strength between copper atoms. To accomplish this, we map the total energies of the various spin configurations γ onto those of the nearest-neighbor Heisenberg Hamiltonian^{67,68}, written as

$$\mathcal{H} = \sum_{\langle i < j \rangle} J_{ij} \mathbf{S}_i \cdot \mathbf{S}_j. \quad (11)$$

Here $i(j)$ indexes the magnetic ion lattice positions, S_i is the local magnetic moment on lattice site i . J_{ij} is the nearest-neighbor exchange interaction strength, with the symmetry properties of $J_{ij} = J_{ji}$. Assuming a fully isotropic bond independent model and separating in- and out-of-plane components, we find

$$J_{\perp} = \frac{(E^{\uparrow\uparrow} + E^{\downarrow\downarrow}) - (E^{\uparrow\downarrow} + E^{\downarrow\uparrow})}{4 \cdot 4 \langle S \rangle^2}, \quad (12)$$

$$J_{\parallel} = \frac{(E^{\uparrow\uparrow} + E^{\downarrow\downarrow}) - (E^{\uparrow\downarrow} + E^{\downarrow\uparrow})}{4 \cdot 2 \langle S \rangle^2}. \quad (13)$$

Using our SCAN ground state total energies, $J_{\perp} = 0.47$ meV, while $J_{\parallel} = -1.67$ meV, with a self-consistent copper magnetic moment of $0.73\mu_B$. The magnetic exchange values are quite small, consistent with the large in-plane and out-of-plane Cu-Cu distance of 9.66 Å and 7.23 Å, respectively. Additionally, the neighboring oxygen atoms exhibit a small but non-zero magnetic moment of $\sim \pm 0.03\mu_B$, while the magnetic moments of Pb and P atoms are effectively zero ($\sim \pm 0.005\mu_B$), suggesting the oxygens form a weak bridge to help facilitate the exchange interactions between Cu atoms.

The dichotomy of localized and extended states finds an intersection in flat band systems. Flat bands may arise from localized impurity levels, low dimensional sub-units of solids, or geometric frustration in lattices, but the

physical underpinnings are quite different. Despite the appearance of a flat band at the Fermi level in copper-doped Pb-apatite, the band character is heavily copper, suggesting these states are trivial impurity-like states. Furthermore, in comparing to our RPA and magnetic exchange coupling analysis, the weak coupling parameters indicate the magnetic moments are quite local with little connection to their neighboring magnetic ion sites, allowing for multiple magnetic ground state that are effectively degenerate. This suggests the RPA results should be interpreted as stemming from local copper atoms that are isolated and do not significantly couple with its environment, thereby generating a multiplicity of seemingly degenerate ground states. To corroborate this picture we attempted to calculate the next-nearest and next-next-nearest exchange parameters, but we could not accurately converge our total energies below ~ 0.1 meV scale, thereby giving more credence to localized impurity moment picture.

IV. CONCLUSION

In summary, we have performed density functional theory and RPA calculations of the electronic band structure, magnetic instabilities, and magnetic exchange parameters of copper-doped $\text{Pb}_{10}\text{P}_6\text{O}_{25}$. We reveal an extremely flat half-filled band at the Fermi level composed of hybridized Cu- d and O- p states where upon adding on-site Coulomb interactions, a fluctuating incommensurate AFM instability is predicted arising from Cu- d_{yz} and $-d_{xz}$ orbitals. However, despite the alluring nature of the flat band, the weak nearest-neighbor exchange coupling combined with the RPA analysis, suggest the magnetism in $\text{Pb}_9\text{CuP}_6\text{O}_{25}$ is localized on the impurity copper site.

DECLARATION OF COMPETING INTEREST

The authors declare that they have no known competing financial interests or personal relationships that could have appeared to influence the work reported in this paper.

ACKNOWLEDGMENTS

This work was carried out under the auspices of the U.S. Department of Energy (DOE) National Nuclear Security Administration under Contract No. 89233218CNA000001. It was supported by the LANL LDRD Program, and in part by the Center for Integrated Nanotechnologies, a DOE BES user facility, in partnership with the LANL Institutional Computing Program for computational resources. Additional computations were performed at the National Energy Research Scientific Computing Center (NERSC), a U.S. Department of Energy Office of Science User Facility located

at Lawrence Berkeley National Laboratory, operated un-

der Contract No. DE-AC02-05CH11231 using NERSC award ERCAP0028014.

- ¹ Yonglong Xie, Andrew T Pierce, Jeong Min Park, Daniel E Parker, Eslam Khalaf, Patrick Ledwith, Yuan Cao, Seung Hwan Lee, Shaowen Chen, Patrick R Forrester, et al. Fractional chern insulators in magic-angle twisted bilayer graphene. *Nature*, 600(7889):439–443, 2021.
- ² Jiaqi Cai, Eric Anderson, Chong Wang, Xiaowei Zhang, Xiaoyu Liu, William Holtzmann, Yinong Zhang, Fengren Fan, Takashi Taniguchi, Kenji Watanabe, et al. Signatures of fractional quantum anomalous hall states in twisted mote2. *Nature*, 622(7981):63–68, 2023.
- ³ Heonjoon Park, Jiaqi Cai, Eric Anderson, Yinong Zhang, Jiayi Zhu, Xiaoyu Liu, Chong Wang, William Holtzmann, Chaowei Hu, Zhaoyu Liu, et al. Observation of fractionally quantized anomalous hall effect. *Nature*, 622(7981):74–79, 2023.
- ⁴ Yuan Cao, Valla Fatemi, Shiang Fang, Kenji Watanabe, Takashi Taniguchi, Efthimios Kaxiras, and Pablo Jarillo-Herrero. Unconventional superconductivity in magic-angle graphene superlattices. *Nature*, 556(7699):43–50, 2018.
- ⁵ Jeong Min Park, Yuan Cao, Kenji Watanabe, Takashi Taniguchi, and Pablo Jarillo-Herrero. Tunable strongly coupled superconductivity in magic-angle twisted trilayer graphene. *Nature*, 590(7845):249–255, 2021.
- ⁶ Haidong Tian, Xueshi Gao, Yuxin Zhang, Shi Che, Tianyi Xu, Patrick Cheung, Kenji Watanabe, Takashi Taniguchi, Mohit Randeria, Fan Zhang, et al. Evidence for dirac flat band superconductivity enabled by quantum geometry. *Nature*, 614(7948):440–444, 2023.
- ⁷ Linda Ye, Shiang Fang, Mingu Kang, Josef Kaufmann, Yonghun Lee, Caolan John, Paul M Neves, SY Frank Zhao, Jonathan Denlinger, Chris Jozwiak, et al. Hopping frustration-induced flat band and strange metallicity in a kagome metal. *Nature Physics*, 20(4):610–614, 2024.
- ⁸ Jianwei Huang, Lei Chen, Yuefei Huang, Chandan Setty, Bin Gao, Yue Shi, Zhaoyu Liu, Yichen Zhang, Turgut Yilmaz, Elio Vescovo, et al. Non-fermi liquid behaviour in a correlated flat-band pyrochlore lattice. *Nature Physics*, 20(4):603–609, 2024.
- ⁹ Jia-Xin Yin, Songtian S Zhang, Guoqing Chang, Qi Wang, Stepan S Tsirkin, Zurab Guguchia, Biao Lian, Huibin Zhou, Kun Jiang, Ilya Belopolski, et al. Negative flat band magnetism in a spin-orbit-coupled correlated kagome magnet. *Nature Physics*, 15(5):443–448, 2019.
- ¹⁰ Zhiyong Lin, Jin-Ho Choi, Qiang Zhang, Wei Qin, Seho Yi, Pengdong Wang, Lin Li, Yifan Wang, Hui Zhang, Zhe Sun, et al. Flatbands and emergent ferromagnetic ordering in fe 3 sn 2 kagome lattices. *Physical review letters*, 121(9):096401, 2018.
- ¹¹ Jia-Xin Yin, Songtian S Zhang, Hang Li, Kun Jiang, Guoqing Chang, Bingjing Zhang, Biao Lian, Cheng Xiang, Ilya Belopolski, Hao Zheng, et al. Giant and anisotropic many-body spin-orbit tunability in a strongly correlated kagome magnet. *Nature*, 562(7725):91–95, 2018.
- ¹² G Bouzerar. Flat band induced room-temperature ferromagnetism in two-dimensional systems. *Physical Review B*, 107(18):184441, 2023.
- ¹³ Sukbae Lee, Jihoon Kim, Hyun-Tak Kim, Sungyeon Im, SooMin An, and Keun Ho Auh. Superconductor $\text{Pb}_{10-x}\text{Cu}_x(\text{PO}_4)_6\text{O}$ showing levitation at room temperature and atmospheric pressure and mechanism. *arXiv preprint arXiv:2307.12037*, 2023.
- ¹⁴ Sukbae Lee, Ji-Hoon Kim, and Young-Wan Kwon. The first room-temperature ambient-pressure superconductor. *arXiv preprint arXiv:2307.12008*, 2023.
- ¹⁵ Kapil Kumar, NK Karn, and VPS Awana. Synthesis of possible room temperature superconductor LK-99: $\text{Pb}_9\text{Cu}(\text{PO}_4)_6\text{O}$. *Superconductor Science and Technology*, 36(10):10LT02, 2023.
- ¹⁶ Li Liu, Ziang Meng, Xiaoning Wang, Hongyu Chen, Zhiyuan Duan, Xiaorong Zhou, Han Yan, Peixin Qin, and Zhiqi Liu. Semiconducting transport in $\text{Pb}_{10-x}\text{Cu}_x(\text{PO}_4)_6\text{O}$ sintered from Pb_2SO_5 and Cu_3P . *Advanced Functional Materials*, 33(48):2308938, 2023.
- ¹⁷ Ivan Timokhin, Chuhongxu Chen, Ziwei Wang, Qian Yang, and Artem Mishchenko. Synthesis and characterisation of lk-99. *arXiv preprint arXiv:2308.03823*, 2023.
- ¹⁸ Gohil S Thakur, Manuel Schulze, and Michael Ruck. On the synthesis methodologies to prepare ‘ $\text{Pb}_9\text{Cu}(\text{PO}_4)_6\text{O}$ ’: Phase, composition, magnetic analysis and absence of superconductivity. *Superconductor Science and Technology*, 37(1):015013, 2023.
- ¹⁹ H Singh, A Gautam, M Singh, P Saha, P Kumar, P Das, M Lamba, K Yadav, PK Mishra, S Patnaik, et al. On the experimental evidence for possible superconductivity in lk99. *arXiv preprint arXiv:2308.06589*, 2023.
- ²⁰ Kaizhen Guo, Yuan Li, and Shuang Jia. Ferromagnetic hall levitation of lk-99-like synthetic samples. *Science China Physics, Mechanics & Astronomy*, 66(10):107411, 2023.
- ²¹ Hao Wu, Li Yang, Bichen Xiao, and Haixin Chang. Successful growth and room temperature ambient-pressure magnetic levitation of lk-99. *arXiv preprint arXiv:2308.01516*, 2023.
- ²² Prashant K Jain. Superionic phase transition of copper (i) sulfide and its implication for purported superconductivity of lk-99. *The Journal of Physical Chemistry C*, 127(37):18253–18255, 2023.
- ²³ Shilin Zhu, Wei Wu, Zheng Li, and Jianlin Luo. First order transition in $\text{Pb}_{10-x}\text{Cu}_x(\text{PO}_4)_6\text{O}$ ($0.9 < x < 1.1$) containing Cu_2S . *arXiv preprint arXiv:2308.04353*, 2023.
- ²⁴ Thacien Habamahoro, Trevor Bontke, Meiraba Chirrom, Zheng Wu, JM Bao, LZ Deng, and CW Chu. Replication and study of anomalies in lk-99—the alleged ambient-pressure, room-temperature superconductor. *Superconductor Science and Technology*, 37(4):045004, 2024.
- ²⁵ Kapil Kumar, Navneet Kumar Karn, Yogesh Kumar, and VPS Awana. Absence of superconductivity in lk-99 at ambient conditions. *ACS omega*, 8(44):41737–41743, 2023.
- ²⁶ J Cabezas-Escares, NF Barrera, C Cardenas, and F Munoz. Theoretical insight on the lk-99 material. *arXiv preprint arXiv:2308.01135*, 2023.
- ²⁷ Hanbit Oh and Ya-Hui Zhang. S-wave pairing in a two-orbital tJ model on triangular lattice: possible application

- to $\text{Pb}_{10-x}\text{Cu}_x(\text{PO}_4)_6\text{O}$. [arXiv preprint arXiv:2308.02469](#), 2023.
- ²⁸ Omid Tavakol and Thomas Scaffidi. Minimal model for the flat bands in copper-substituted lead phosphate apatite. [arXiv preprint arXiv:2308.01315](#), 2023.
- ²⁹ Sinéad M Griffin. Origin of correlated isolated flat bands in copper-substituted lead phosphate apatite. [arXiv preprint arXiv:2307.16892](#), 2023.
- ³⁰ Rafal Kurlito, Stephan Lany, Dimitar Pashov, Swagata Acharya, Mark van Schilfhaarde, and Daniel S Dessau. Pb-apatite framework as a generator of novel flat-band CuO based physics, including possible room temperature superconductivity. [arXiv preprint arXiv:2308.00698](#), 2023.
- ³¹ Ning Mao, Nikolai Peshcherenko, and Yang Zhang. Wannier functions, minimal model and charge transfer in $\text{Pb}_9\text{CuP}_6\text{O}_{25}$. [arXiv preprint arXiv:2308.05528](#), 2023.
- ³² Hua Bai, Jianrong Ye, Lei Gao, Chunhua Zeng, and Wuming Liu. Semiconductivity induced by spin-orbit coupling in $\text{Pb}_9\text{Cu}(\text{PO}_4)_6\text{O}$. *Scientific Reports*, 13(1):21085, 2023.
- ³³ Jiahong Shen, Dale Gaines, Shima Shahabfar, Zhi Li, Dohun Kang, Sean Griesemer, Adolfo Salgado-Casanova, Tzu-chen Liu, Chang-Ti Chou, Yi Xia, et al. Phase Stability of Lead Phosphate Apatite $\text{Pb}_{10-x}\text{Cu}_x(\text{PO}_4)_6\text{O}$, $\text{Pb}_{10-x}\text{Cu}_x(\text{PO}_4)_6(\text{OH})_2$ ($x=0, 1$), and $\text{Pb}_8\text{Cu}_2(\text{PO}_4)_6$. *Chemistry of Materials*, 36(1):275–285, 2023.
- ³⁴ Hari Paudyal, Michael E Flatté, and Durga Paudyal. Implications of the electron-phonon coupling in $\text{CuPb}_9(\text{PO}_4)_6\text{O}$ for superconductivity: An ab initio study. *Physical review materials*, 8(1):L011801, 2024.
- ³⁵ Ran Liu, Ting Guo, Jiajun Lu, Junfeng Ren, and Tianxing Ma. Different phase leads to different transport behavior in $\text{Pb}_9\text{Cu}(\text{PO}_4)_6\text{O}$ compounds. [arXiv preprint arXiv:2308.08454](#), 2023.
- ³⁶ Bishnu Karki, Kai Chen, and Pavan Hosur. Emergence of weyl points due to spin orbit coupling in lk-99. [arXiv preprint arXiv:2402.18588](#), 2024.
- ³⁷ Hongyang Wang, Yao Yao, Ke Shi, Yijing Zhao, Hao Wu, Zhixing Wu, Zhihui Geng, Shufeng Ye, and Ning Chen. Possible meissner effect near room temperature in copper-substituted lead apatite. [arXiv preprint arXiv:2401.00999](#), 2024.
- ³⁸ Hongyang Wang, Hao Wu, Ning Chen, Xianfeng Qiao, Ling Wang, Zhixing Wu, Zhihui Geng, Weiwei Xue, Shufeng Ye, and Yao Yao. Observation of diamagnetic strange-metal phase in sulfur-copper codoped lead apatite. [arXiv preprint arXiv:2403.11126](#), 2024.
- ³⁹ Yi Jiang, Scott B Lee, Jonah Herzog-Arbeitman, Jibin Yu, Xiaolong Feng, Haoyu Hu, Dumitru Călugăru, Parker S Brodale, Eoghan L Gormley, Maia G Vergniory, et al. $\text{Pb}_9\text{Cu}(\text{PO}_4)_6(\text{OH})_2$: Phonon bands, localized flat-band magnetism, models, and chemical analysis. *Physical Review B*, 108(23):235127, 2023.
- ⁴⁰ Martin Braß, Liang Si, and Karsten Held. Weyl points and spin-orbit coupling in copper-substituted lead phosphate apatite. *Physical Review B*, 109(8):085103, 2024.
- ⁴¹ Moritz M Hirschmann and Johannes Mitscherling. Symmetry-enforced double weyl points, multiband quantum geometry, and singular flat bands of doping-induced states at the fermi level. *Physical Review Materials*, 8(1):014201, 2024.
- ⁴² Niklas Witt, Liang Si, Jan M Tomczak, Karsten Held, and Tim O Wehling. No superconductivity in $\text{Pb}_9\text{Cu}_1(\text{PO}_4)_6\text{O}$ found in orbital and spin fluctuation exchange calculations. *SciPost Physics*, 15(5):197, 2023.
- ⁴³ Dmitry M Korotin, Dmitry Y Novoselov, Alexey O Shorikov, Vladimir I Anisimov, and Artem R Oganov. Electronic correlations in the ultranarrow energy band compound $\text{pb}_9\text{cu}(\text{po}_4)_6\text{o}$: A dft+ dmft study. *Physical Review B*, 108(24):L241111, 2023.
- ⁴⁴ Changming Yue, Viktor Christiansson, and Philipp Werner. Correlated electronic structure of $\text{pb}_{10-x}\text{cu}_x(\text{po}_4)_6\text{o}$. *Physical Review B*, 108(20):L201122, 2023.
- ⁴⁵ Sun-Woo Kim, Kristjan Haule, Gheorghe Lucian Pascut, and Bartomeu Monserrat. Non-fermi liquid to charge-transfer mott insulator in flat bands of copper-doped lead apatite. *Materials Horizons*, 11(22):5622–5630, 2024.
- ⁴⁶ Yang Sun, Kai-Ming Ho, and Vladimir Antropov. Metallization and spin fluctuations in cu-doped lead apatite. *Physical Review Materials*, 7(11):114804, 2023.
- ⁴⁷ Lorenzo Celiberti, Lorenzo Varrassi, and Cesare Franchini. $\text{Pb}_9\text{cu}(\text{po}_4)_6\text{o}$ is a charge-transfer semiconductor. *Physical Review B*, 108(20):L201117, 2023.
- ⁴⁸ Dimitar Pashov, Swagata Acharya, Stephan Lany, Daniel S Dessau, and Mark van Schilfhaarde. Multiple slater determinants and strong spin-fluctuations as key ingredients of the electronic structure of electron-and hole-doped $\text{pb}_{10-x}\text{cu}_x(\text{po}_4)_6\text{o}$. [arXiv preprint arXiv:2308.09900](#), 2023.
- ⁴⁹ Makoto Shimizu, Junya Otsuki, and Harald O Jeschke. Magnetic fluctuations in $\text{pb}_9\text{cu}(\text{po}_4)_6\text{o}$. *Physical Review B*, 108(20):L201105, 2023.
- ⁵⁰ Peter E Blöchl. Projector augmented-wave method. *Physical review B*, 50(24):17953, 1994.
- ⁵¹ Georg Kresse and Daniel Joubert. From ultrasoft pseudopotentials to the projector augmented-wave method. *Physical review b*, 59(3):1758, 1999.
- ⁵² Georg Kresse and Jürgen Furthmüller. Efficient iterative schemes for ab initio total-energy calculations using a plane-wave basis set. *Physical review B*, 54(16):11169, 1996.
- ⁵³ Georg Kresse and JJPRB Hafner. Ab initio molecular dynamics for open-shell transition metals. *Physical Review B*, 48(17):13115, 1993.
- ⁵⁴ Jianwei Sun, Adrienn Ruzsinszky, and John P Perdew. Strongly constrained and appropriately normed semilocal density functional. *Physical Review Letters*, 115(3):036402, 2015.
- ⁵⁵ Jianwei Sun, Richard C Remsing, Yubo Zhang, Zhaoru Sun, Adrienn Ruzsinszky, Haowei Peng, Zenghui Yang, Arpita Paul, Umesh Waghmare, Xifan Wu, et al. Accurate first-principles structures and energies of diversely bonded systems from an efficient density functional. *Nature chemistry*, 8(9):831–836, 2016.
- ⁵⁶ Sergey V Krivovichev and Peter C Burns. Crystal chemistry of lead oxide phosphates: crystal structures of $\text{pb}_4\text{o}(\text{po}_4)_2$, $\text{pb}_8\text{o}_5(\text{po}_4)_2$ and $\text{pb}_{10}(\text{po}_4)_6\text{o}$. *Zeitschrift für Kristallographie-Crystalline Materials*, 218(5):357–365, 2003.
- ⁵⁷ Junwen Lai, Jiangxu Li, Peitao Liu, Yan Sun, and Xing-Qiu Chen. First-principles study on the electronic structure of $\text{pb}_{10-x}\text{cu}_x(\text{po}_4)_6\text{o}$ ($x=0, 1$). *Journal of Materials Science & Technology*, 171:66–70, 2024.
- ⁵⁸ Malte Schüler, Oleg E Peil, Gernot J Kraberger, Ronald Pordzik, Martijn Marsman, Georg Kresse, Tim O Wehling, and Markus Aichhorn. Charge self-consistent many-body corrections using optimized projected localized orbitals. *Journal of Physics: Condensed Matter*, 30(47):475901, 2018.

- ⁵⁹ Giovanni Pizzi, Valerio Vitale, Ryotaro Arita, Stefan Blügel, Frank Freimuth, Guillaume Géranton, Marco Gibertini, Dominik Gresch, Charles Johnson, Takashi Koretsune, et al. Wannier90 as a community code: new features and applications. *Journal of Physics: Condensed Matter*, 32(16):165902, 2020.
- ⁶⁰ Christopher Lane, Ruiqi Zhang, Bernardo Barbiellini, Robert S Markiewicz, Arun Bansil, Jianwei Sun, and Jian-Xin Zhu. Competing incommensurate spin fluctuations and magnetic excitations in infinite-layer nickelate superconductors. *Communications Physics*, 6(1):90, 2023.
- ⁶¹ Christopher Lane and Jian-Xin Zhu. Identifying topological superconductivity in two-dimensional transition-metal dichalcogenides. *Physical Review Materials*, 6(9):094001, 2022.
- ⁶² P Puphal, MYP Akbar, M Hepting, E Goering, M Isobe, AA Nugroho, and B Keimer. Single crystal synthesis, structure, and magnetism of pb10- xcux (po4) 6o. *APL Materials*, 11(10), 2023.
- ⁶³ Chang Liu, Wenxin Cheng, Xiaoxiao Zhang, Juan Xu, Jiaxin Li, Qiuyan Shi, Changhong Yuan, Li Xu, Honglin Zhou, Shilin Zhu, et al. Phases and magnetism at microscale in compounds containing nominal pb 10- x cu x (po 4) 6 o. *Physical Review Materials*, 7(8):084804, 2023.
- ⁶⁴ Pinyuan Wang, Xiaoqi Liu, Jun Ge, Chengcheng Ji, Hao-ran Ji, Yanzhao Liu, Yiwen Ai, Gaoxing Ma, Shichao Qi, and Jian Wang. Ferromagnetic and insulating behavior in both half magnetic levitation and non-levitation lk-99 like samples. *Quantum Frontiers*, 2(1):10, 2023.
- ⁶⁵ Toru Moriya. *Spin fluctuations in itinerant electron magnetism*, volume 56. Springer Science & Business Media, 2012.
- ⁶⁶ Léon Van Hove. The occurrence of singularities in the elastic frequency distribution of a crystal. *Physical Review*, 89(6):1189, 1953.
- ⁶⁷ Hongjun Xiang, Changhoon Lee, Hyun-Joo Koo, Xingao Gong, and Myung-Hwan Whangbo. Magnetic properties and energy-mapping analysis. *Dalton Transactions*, 42(4): 823–853, 2013.
- ⁶⁸ Jian-Xin Zhu, Rong Yu, Hangdong Wang, Liang L Zhao, MD Jones, Jianhui Dai, Elihu Abrahams, E Morosan, Minghu Fang, and Qimiao Si. Band narrowing and mott localization in iron oxychalcogenides la 2 o 2 fe 2 o (se, s) 2. *Physical review letters*, 104(21):216405, 2010.